Real-time and Cost-efficient Indoor Localization and Mapping Solution for Emergency Response Applications

Hamdy Elsayed[1], Ahmed Shaker[1]

[1] Toronto Metropolitan University, Department of Civil Engineering,
Toronto, ON, Canada - Hamdy.Elsayed@TorontoMU.ca

Keywords: Indoor, LiDAR, SLAM, Emergency, Real-time, Mapping.

Abstract

In GNSS-denied environments such as indoor and underground locations, real-time mapping and navigation are paramount, especially for emergency response scenarios like search and rescue or building evacuations. First responders rely on accurate maps of entrances and exits to prevent disorientation. This research addresses the challenges posed by the absence of GNSS signals and the need for high-performance data processing by developing a cost-effective multi-sensor system for real-time indoor mapping. The system incorporates consumer-grade technologies, including 2D LiDAR, RGB-D cameras, and MEMS-based IMU. It utilizes the Google Cartographer SLAM engine to generate real-time 2D raster maps and stream position and orientation data at 200 poses per second, ensuring continuous poses feed while minimizing latency. The resulting maps are continuously being optimized using a loop-closing algorithm to reduce drift and maintain the trajectory integrity. The system was validated in both real-time and post-processing configurations, the proposed system demonstrates promising consistency and repeatability according to the verification results furnished in this research paper. The data collection and processing times with this system are significantly reduced compared to static LiDAR systems, without the need for high-end computing resources. This research underscores the benefits of using inexpensive sensors and components, providing an efficient solution for indoor mapping and navigation in emergency scenarios.

1. Introduction

Indoor mapping presents unique challenges due to the absence or obstruction of GNSS signals. Existing indoor mobile mapping systems that operate in GNSS-denied environments often utilize low-cost sensors, such as MEMS-based IMUs, RGB-D cameras, and mapping- or industrial-grade LiDAR sensors (Chiang et al., 2021). These sensors provide relatively lower accuracy than high-end sensors, which may not meet the accuracy requirements of specific applications but could be a good fit for underground environments, building navigation, and emergency response operations, which do not require high accuracy and precision.

Therefore, there is a need to develop mobile mapping systems that address the challenges of high accuracy and precision outdoor mapping, as well as indoor mapping systems in GNSS-denied environments with a necessity for real-time capabilities for some applications (Elhashash et al., 2022). These systems should be cost-effective, accessible, and capable of capturing geospatial data with the highest possible accuracy and precision, suitable for various applications.

A key motivation for research in this area is the potential for mobile mapping systems to enhance the efficiency and effectiveness of various applications. For instance, real-time mapping in GNSS-denied environments, such as indoor spaces, can enable navigation and tracking in complex environments, improving emergency operations' response time and effectiveness. Furthermore, digital twin modelling involves creating virtual replicas of physical environments and can benefit from mobile mapping systems to capture accurate and up-to-date data for creating and updating digital twins in real-time. These digital twins can be used for various applications, such as urban planning, facility management, and disaster management, leading to more informed decision-making and improved outcomes (Xue et al., 2020).

However, significant challenges in the development of mobile mapping systems need to be addressed. One of the main challenges is the cost associated with these systems, including the specialized sensors and technologies required for high accuracy and precision mapping. The cost factor often limits the accessibility of mobile mapping systems to a wide range of users and applications (Elhashash et al., 2022). Additionally, latency, or the time it takes for the system to process and display the collected data, can be challenging, especially in real-time applications like navigation, where even minor delays can be disruptive (Lv et al., 2020). Finally, the complexity of mobile mapping systems, with multiple components and technologies that need to be integrated and calibrated, poses challenges in system design and operation.

The proposed system in this research contains two orthogonal 2D LiDAR sensors, a Microsoft Kinect camera, and an industrial-grade IMU. The system sensors are all mounted on a moving cart. All the sensors are connected to a hosting computer that runs the Linux Ubuntu and hosts A Robotic Operating System (ROS) Melodic version (Quigley et al., 2009). Each sensor is connected to the hosting computer and streams its real-time data through a ROS driver that listens to the sensors' stream and broadcasts the sensor data in a standard ROS message format.

Google Cartographer is used for SLAMing the LiDAR data and generating the best trajectory estimate and 3D point clouds. The package includes several ROS nodes, each performing a specific task in the SLAM pipeline. For example, there is a node for subscribing to point cloud and IMU data, a node for performing loop closure detection, and a node for generating the final map (Xu et al., 2017). One important challenge in LiDAR SLAM is drift, the error that accumulates over time as the LiDAR sensor moves through the environment. This error can cause the map to become distorted and less accurate, making it difficult to use it for navigation or other tasks.

Researchers and developers have developed various techniques and algorithms to address the drift problem in LiDAR SLAM [103] (Di Filippo et al., 2018). These include methods for filtering and smoothing the LiDAR data to reduce noise and errors, as well as algorithms for tracking the motion of the LiDAR sensor more accurately, called motion compensation in literature (Lv et al., 2020).

The novelty of this system is built on multiple facts against the other comparable state-of-the-art industrial systems, and it outperformed them in terms of cost and handiness. First, the sensors used are extraordinarily inexpensive and not intended by their manufacturers to be used in localization and mapping. Secondly, the system uses a combination of sensors that was not presented in previous research. Thirdly, the system is relatively lightweight and compact, allowing room to be used in emergency response applications such as search and rescue operations by attaching the system to the first responder's suit or helmet.

2. System Components

The overall system hardware design is shown in Figure 1. The system consists of two 2D RPLiDAR Sensors placed orthogonally to each other, one oriented to the horizontal plane and parallel to the ground, and the second plane makes a 90-degree angle with the horizontal plane. Moreover, the system is equipped with a basic PhidgetSpatial IMU. It is tightly fixed underneath the horizontal LiDAR to allow the system to determine the levelling angles for the Horizontal LiDAR and shorten the SLAM convergence time by providing an initial approximation for the orientation angles.

The two LiDAR sensors and the IMU are both fixed on a custom-made monopod to keep them all rigidly coupled all the time. In addition to the RPLiDAR sensors, this system is equipped with an MS Kinect v1 depth camera, mainly used to enrich the point cloud with further dense points. It is mounted on a plate vertically separated by 124 cm from the horizontal LiDAR, facing forward to the direction of movement. All the sensors are mounted on a moving cart with omnidirectional wheels for smooth manoeuvrability in tight spaces.

The only sensor that requires an external power supply is the Kinect. That is why a battery is attached to the cart to power up the Kinect depth camera. In contrast, RPLiDAR and PhidsgetSpatial sensors get the required power from the operating computer USB ports. Finally, the screen faces backward to give a good viewpoint to the system operator to monitor the data streams and the real-time mapping processes during the data acquisition time.

Figure 1. The Overall System Design

The overall software architecture for the system is shown in Figure 2. The software design does not require any external time synchronization. Every sensor gets its data time-stamped by the operating system as soon as it is acknowledged on the communication interface of ROS.

A dedicated driver is pre-installed on ROS to establish communication with every sensor and stream the data within ROS in a standard message format.

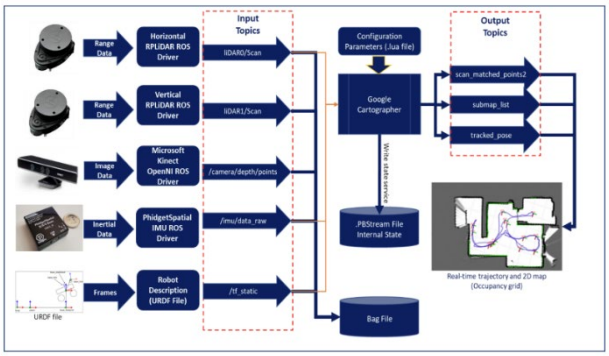

Figure 2. The Overall Software Architecture

Every standard message is broadcasted on ROS on a unique topic to ease the process of receiving those messages from the listeners. The listeners are software packages or ROS nodes waiting for the sensor data to implement their routines and perform real-time processing. One of the critical listeners in this system is Google Cartographer, the software package responsible for gathering the sensor data and implementing the SLAM method in real time to estimate the position and orientation, AKA—pose of the sensors and the moving platform.

Google Cartographer broadcasts the pose of the sensors and a 2D map in real-time on three topics in the red dotted box named “output topics” in Figure 2. A real-time map viewer listens to those output topics to instantly display the map and trajectory. This map viewer is a built-in software package in ROS called Rviz. To further process the data offline and produce a complete 3D map which is the Point cloud, all the raw sensor data are saved in a particular file format named Bag file, where ROS can store a massive amount of sensor data and access them efficiently at any time.

In addition, all the poses are exported at the end of the SLAM process in a PBStream format to be used in georeferencing the sensor data and building the final point cloud data.

3. Frames of Reference

This section illustrates the georeferencing through Equation 1 and Equation 2 for the two Lidar sensors. Any vector in this equation system represents a 3D coordinate in one of the frames of reference. Any vector with a subscript only represents 3D coordinates in a particular frame defined by the subscript. Any vector with both superscript and subscript represents a shift from the subscript frame to the superscript frame. Any Rotation matrix (R) is a right-handed rotation matric from the subscript frame to the superscript frame (Velas et al., 2019).

The system includes five sensors and nine frames of reference, as shown in Figure 3. The base_link is the reference frame, a virtual static frame attached to the moving platform where the x-axis

looks forward, the y-axis is to the left, and the z-axis is in the up direction. laser0 is coaligned with base_link, and all the transformation parameters between laser0 and the reference frame are set to zero.

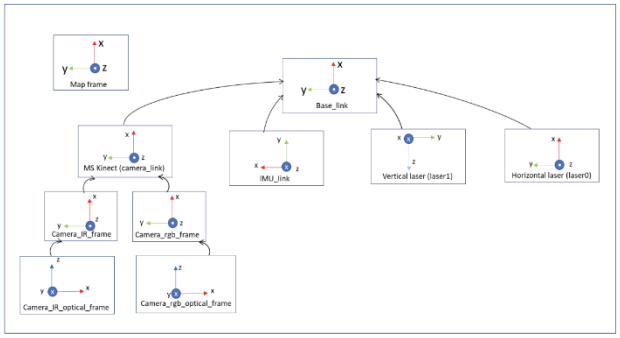

Figure 3. Frames of References

The laser0, imu_link, and camera_link frames are all related to the base_link frame by applying the measured transformation parameters, including translation in the reference frame in the x, y, and z directions. Also, it includes the rotation angles, roll, pitch, and yaw to rotate every child frame to the parent frame.

Table 1 illustrates all the translation and rotation parameters to transform from one frame to the other. Kinect OpenNI ROS driver publishes the transformation parameters for camera_depth_frame, camera_rgb_frame, camera_optical_depth_frame, and camera_optical_rgb_frame, which are provided by the sensor manufacturer and never change since they represent the internal architecture of the sensors. In contrast, all the other frames' transformation parameters are measured and adjusted by co-registering the sensor data and trying and co-aligning the different sensors' data.

		Meters			Radians		
Frame	**Parent frame**	**x**	**y**	**z**	**Roll**	**Pitch**	**Yaw**
Base_link							
Laser0	Base_link	0	0	0	0	0	0
Laser1	Base_link	0	0.05	-0.09	0	1.570790	3.14159
Imu_link	Base_link	-0.01	-0.005	-0.05	3.141590	0	-1.570796
Camera_link	Base_link	0.127	-0.148	-1.245	0	0	0.035
Camera_depth_frame	Camera_link	0	-0.02	0	0	0	0
Camera_rgb_frame	Camera_link	0	-0.045	0	0	0	0
Camera_depth_optical_frame	Camera_depth_frame	0	0	0	-1.570796	0	-1.570796
Camera_rgb_optical_frame	Camera_rgb_frame	0	0	0	-1.570796	0	-1.570796

Table 1. System Translation and Rotation Parameters

$$\begin{bmatrix} x_p \\ y_p \\ z_p \end{bmatrix}_{map} = \begin{bmatrix} x_{base\_link} \\ y_{base\_link} \\ z_{base\_link} \end{bmatrix}_{map} + R^{map}_{base\_link} \begin{bmatrix} \Delta x \\ \Delta y \\ \Delta z \end{bmatrix}^{base\_link}_{laser0} + R^{map}_{base\_link} R^{base\_link}_{laser0} \begin{bmatrix} x_p \\ y_p \\ z_p \end{bmatrix}_{laser}$$

Equation 1. Georeferencing of Horizontal Lidar

$$\begin{bmatrix} x_p \\ y_p \\ z_p \end{bmatrix}_{map} = \begin{bmatrix} x_{base\_link} \\ y_{base\_link} \\ z_{base\_link} \end{bmatrix}_{map} + R^{map}_{base\_link} \begin{bmatrix} \Delta x \\ \Delta y \\ \Delta z \end{bmatrix}^{base\_link}_{laser1} + R^{map}_{base\_link} R^{base\_link}_{laser1} \begin{bmatrix} x_p \\ y_p \\ z_p \end{bmatrix}_{laser1}$$

Equation 2. Georeferencing of Vertical Lidar

4. System Validation Methodology

To implement the system validation, the developed workflow shown in Figure 4 was followed.

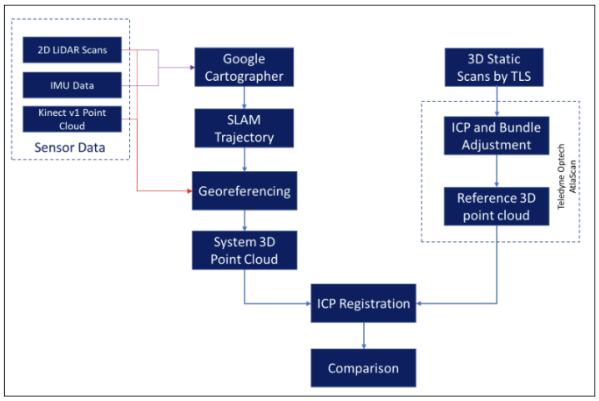

Figure 4. System Validation Workflow

First, Google Cartographer used the configuration file to receive a stream of the horizontal LiDAR scans and the IMU raw measurements during the data acquisition time. The proposed Google Cartographer workflow is used to generate the SLAM trajectory, including the platform sensors' position and orientation. In the post-processing phase, all the range data, including those generated from the LiDAR sensors and the data from Microsoft Kinect, were georeferenced. Once the final point cloud is generated from the Google Cartographer asset writer routine, the validation and verification process can be initiated (Sammartano and Spanò, 2018).

A reference LiDAR data is compared with the system point cloud and evaluates the system's LiDAR data outcomes. To begin the comparison process, survey-grade TLS LiDAR equipment manufactured by Teledyne Optech, namely “Polaris,” was used to collect multiple static LiDAR scans at different locations in the selected site for validation. Then the TLS scans were precisely registered starting with a feature-based registration followed by an ICP registration and bundle adjustment (Pomerleau et al., 2013).

The output of the TLS scan registration is a single reference point cloud that will be used as benchmark data with the proposed system output point cloud. The reference LiDAR data and the proposed system point cloud must be georeferenced to the same coordinate system. Once the data is aligned correctly, the next step is to evaluate the differences between the two point clouds.

The selected site for the system validation is the 3rd floor of the Monetary Times building at Toronto Metropolitan University. Figure 5 depicts the validation site with the locations of the TLS-stations to collect the reference dataset. The overlap between the terrestrial LiDAR stations refers to the extent to which the measurements taken at different stations cover the same area on the ground. This overlap is significant because it creates a more detailed and accurate reference point cloud to be compared with the proposed system’s point cloud

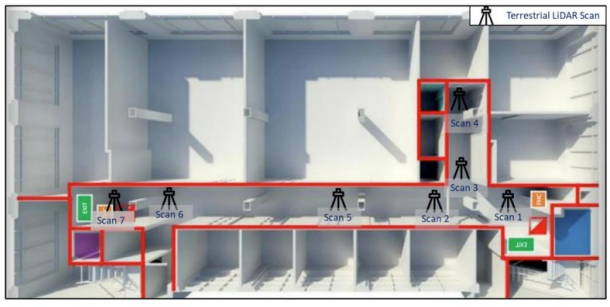

Figure 5. Margin settings for A4 size paper

Teledyne AtlaScan is a powerful software suite that processes and analyzes LiDAR survey data collected by the Teledyne Optech Polaris TLS. This research work leverages AtlaScan based on (Li et al., 2021) to carry out the following processing tasks to register the TLS scan precisely and establish a single reference point cloud:

i. Preprocessing: filters noise, removes outliers, and computes normal vectors.

ii. Coarse Registration: computes a rough alignment between the imported models.

iii. ICP Registration: refines the alignment between any two point clouds

iv. Bundle Adjustment: refines the alignment between all the point clouds The ICP algorithm works by iteratively minimizing the difference between two point clouds to find the best alignment of the point clouds.

The algorithm then uses corresponding points to compute a transformation that aligns the two point clouds as depicted in Figure 6.

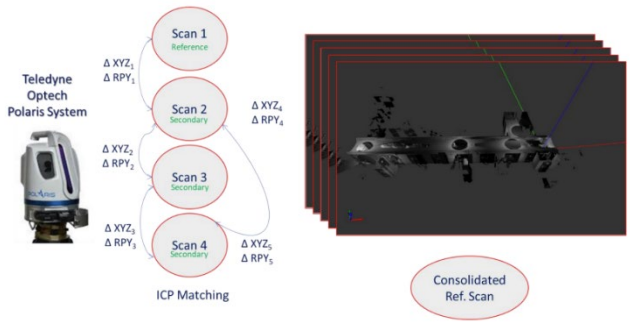

Figure 6. Point Clouds Registration

To collect a system validation dataset, the system platform was moved slowly and steadily to scan the whole 3rd-floor hallways of the Monetary Times Building, and took 12 minutes to cover two hallways one is 27 meters and the other is 7 meters long, and both hallways width is 3 meters width. A one-long loop trajectory was materialized, and then the cart was held standstill at the loop closure point to let the system optimize the trajectory and the submaps using the Global SLAM optimization algorithm of Google Cartographer.

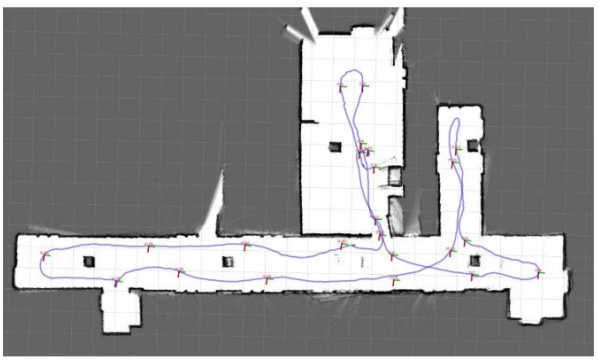

Figure 7. Real-time Generated 2D SLAM Map

Figure 7 depicts the real-time generated 2D map of the collected data of the horizontal sensor along with the trajectory and the origin of each submap. The optimized trajectory has to be exported in a standard Google Cartographer PBStream file to be combined with the raw sensor data and generate the final georeferenced point cloud.

5. Experimental Setup and Results

5.1 The Georeferenced System Data

The final point cloud was built using the adjusted trajectory information and the raw sensor data. It was also claimed that the primary purpose of MS Kinect is to densify the point cloud and fill any gaps in the Lidar data. To visually interpret the added value of using MS Kinect, the final point cloud was generated once without Kinect data, shown in Figure 8; and another point cloud was generated with Kinect data included, as shown in Figure 9.

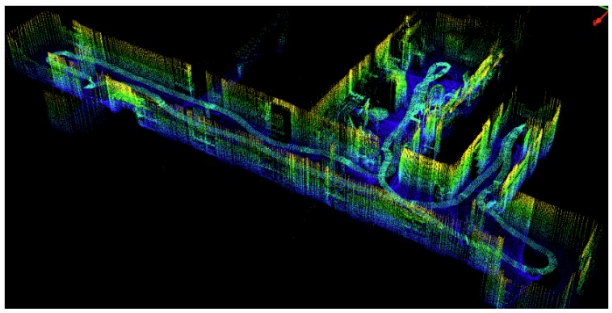

Figure 8. System Point Cloud without Kinect Data

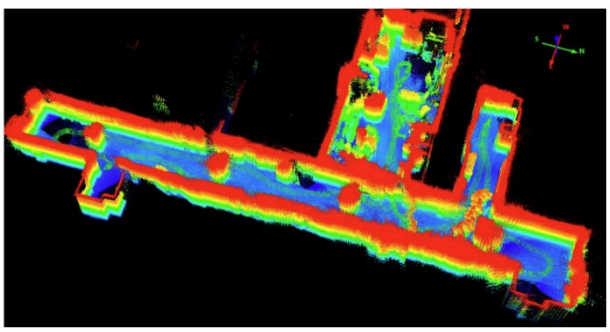

Figure 9. System Point Cloud with Kinect Data

5.2 Preparing the Reference TLS Scans for Validation

To generate a single referenced point cloud to benchmark the system, seven TLS scans have been collected using Teledyne Optech Polaris at different locations to cover the entire 3rd floor of the MON building at TMU. Figure 10 depicts the individual scans collected and viewed by the reflected intensity of the returned signals; most importantly, these scans must be overlapped to ensure the success of the registration process.

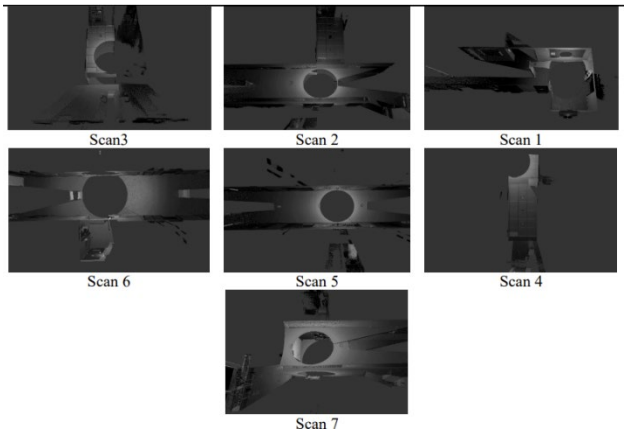

Figure 10. Individual TLS Reference Scans

Once the bundle adjustment process is done on Atlascan software, the adjusted relative position and orientation of each TLS scan are saved and appended to each scan metadata, as shown in Table

	Trans x (meters)	Trans y (meters)	Trans z (meters)	Rot x (degrees)	Rot y (degrees)	Rot z (degrees)
Scan 1	-0.340	0.025	0.002	-0.9108	-0.8454	-62.9316
Scan 2	-4.273	0.584	0.014	-1.4048	-0.3629	-92.7254
Scan 3	-2.624	3.144	0.021	-1.0382	0.0761	-90.4764
Scan 4	-3.521	7.331	-0.061	0.9469	-0.5602	-167.8686
Scan 5	-11.510	1.311	0.031	-1.217	0.874	-137.942
Scan 6	-20.641	2.199	0.051	-1.139	0.799	-122.775
Scan 7	-24.243	2.311	-0.036	0.065	-0.692	119.303

Table 2. Adjusted Position and Orientation of TLS scans

After tuning the necessary translation and rotation transformation parameters to co-register each scan with the reference scan, the individual scans were transformed and georeferenced relative to the coordinate system of the reference scan. The outcome of this process is a homogeneous, consistent reference point cloud where the registration error did not exceed 4 mm across the seven TLS scans.

Figure 11 illustrates the registered TLS scans in a single consolidated reference scan. Each scan was given a unique colour to give a better visual interpretation.

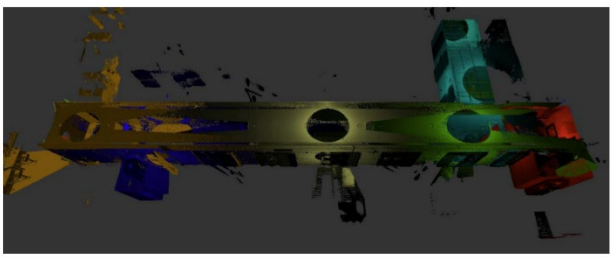

Figure 11. Co-registered TLS Reference Scans

5.3 Registration of the System Point Cloud to the Reference Scan Data

The final step before validating and comparing the system data versus the reference data is to coregister both data in the same coordinate system. Teledyne Optech AtlaScan was used again to do the job through the ICP registration process to resolve the best estimate for translation and rotation to transform the system scan in the reference scan’s coordinate system. The ICP results showed a mean registration error between the point pairs of 2 cm.

6. Experimental Results

The system benchmarking was performed by analysing the point density, accuracy, distribution, and point cloud data profiling. Although the TLS reference scans are very consistent and were precisely registered, it is essential to note that the reference data has some data gaps in circular shapes, as shown in Figure 12 (a).

This is because the reference TLS LiDAR sensor cannot detect targets closer than 1.5 meters from the sensor head due to the saturation of the optical detector. Additionally, the system's point cloud shown in Figure 12 (b) exhibits a fixed pattern of points in light blue due to the presence of a computer shelf on the moving platform in the field of view of the LiDAR sensors during the entire data collection period. This results in the point cloud having an almost aligned pattern with the entire dataset's trajectory.

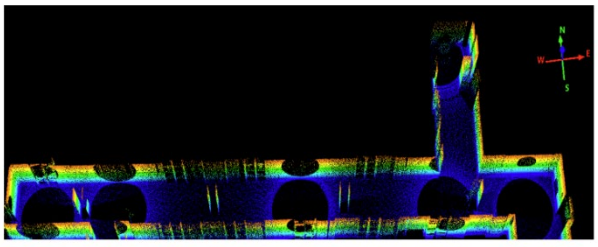

(a) Overall Reference point cloud with the ceiling removed

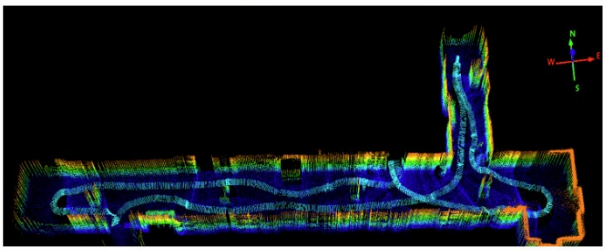

(b) Overall System point cloud with the ceiling removed

Figure 12. Margin settings for A4 size paper

The point distribution refers to the pattern in which the laser pulses are emitted and how they are distributed across the area being scanned. A consistent point distribution ensures that the resulting point cloud is dense and has a uniform coverage of points across the entire area, ensuring that no areas are missed or under-sampled.

The reference point cloud data was found to be very consistent and well distributed except for the circular gaps in the data due to the sensor characteristics. On the other side, the system point cloud is well-distributed across the environment and does not show any data gaps; however, due to the nature of a typical mobile mapping system, the density is not as consistent as in the reference dataset.
The second aspect of benchmarking is built on interpreting the system data resolution. In general, higher-resolution LiDAR data has a more significant number of points and a higher level of detail, while lower-resolution LiDAR data has fewer points and less detail. Figure 13 (a) shows the data resolution obtained from one of the walls, and it depicts all the texture and features on the wall, including windows and doors, and all the bare spots look consistent and homogeneous.

Figure 13 (b) illustrates the resolution obtained from the system data. The level of detail is very close to the reference data, so all the features are clear enough to be distinguished. However, the

sharpness of the features is weaker than the reference data because the reference data features higher density and collects more points per square unit.

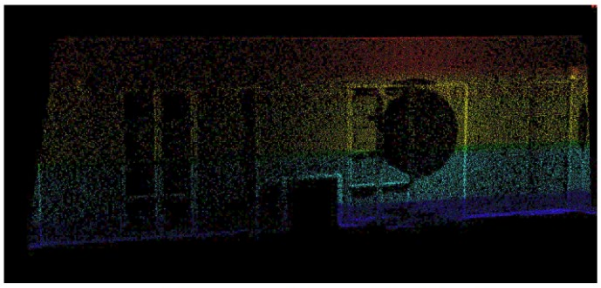

(a) Reference scan wall texture and level of details

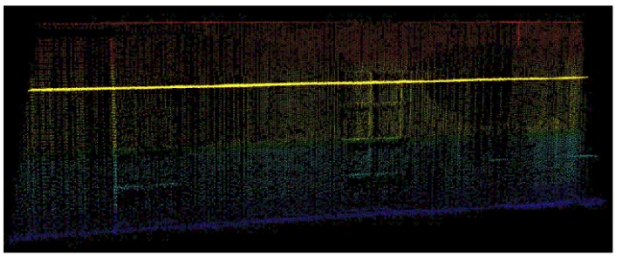

(b) System scan wall texture and level of details

Figure 13. System versus Reference Data Resolution

The third aspect of benchmarking and validating the system data is a comparison based on the data density. Intuitively, the reference data features a higher point density than the reference data since it combines static scans. In each static scan, the LiDAR sensor is placed on a tripod and slowly rotates 360 degrees around its vertical axis while collecting data. This process takes a few minutes to complete and results in a high density of points in the point cloud, which is more than any mobile system could collect by scanning the same environment.

Figure 14 compares the system and reference data in terms of density. The system data has a maximum point density of 14,000 points per square meter, while the reference data has a maximum point density of 916,000 points per square meter. The reference data exhibits high-density metrics in red on almost all the walls. That contrasts the system data, which has only a few red spots and the remaining points in the yellow to blue shade, indicating a lower point density. These results show that the reference data has a much higher point density and more accurate environment representation than the system data.

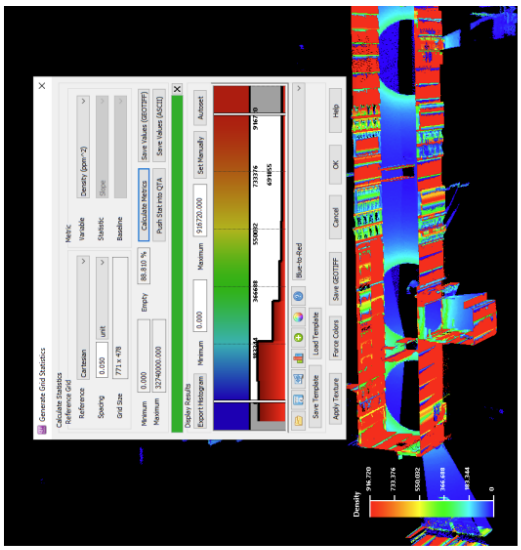

(a) Reference data density (points per square meter)

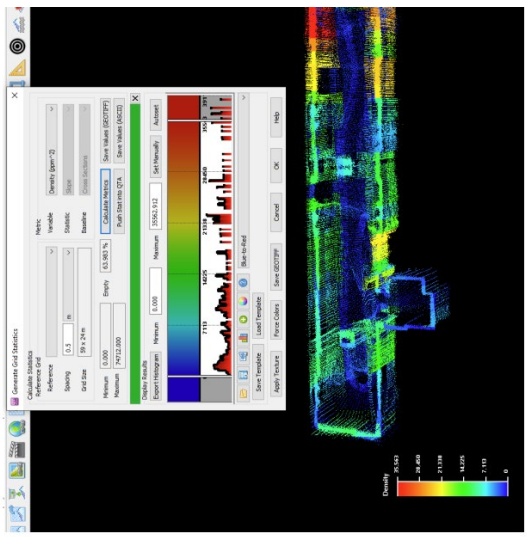

(b) System data density (points per square meter)

Figure 14. System and Reference Data Density Comparison

The fourth aspect of benchmarking involved a comparative analysis of cross-sections derived from the system data and reference data. In total, five cross-section lines were drawn across the corridor of the testing data using the Quick Terrain Modeler visualization tool. Exemplary cross-sections are presented in Figure 15. The examination of these cross-sections revealed that the ground and ceiling alignment was consistent, with an average misclosure of only 2.5 cm observed across the entire dataset.

Furthermore, additional analysis based on the cross-sections. While the reference data featured a wall thickness of approximately 1 cm for the data points, the system data depicted the same wall with a thickness ranging from 9 to 10 cm. This observation suggests that the system data, while relatively accurate and detailed, may not match the precision and level of detail present in the reference data. In a separate investigation, another cross-section of the data was examined. The wall thickness, and the system data exhibited variations ranging from 2.5 to 7 cm while the reference system wall thickness remains the same at 1 cm thickness. To conclude, the comparative analysis of cross-sections between the system and reference data provides insights into the relative accuracy of the system when it is

compared to the reference dataset. While the ground and ceiling are aligned with a little misclosure, differences in wall thicknesses indicate that the reference data, with its higher point density, is likely to be more precise and detailed

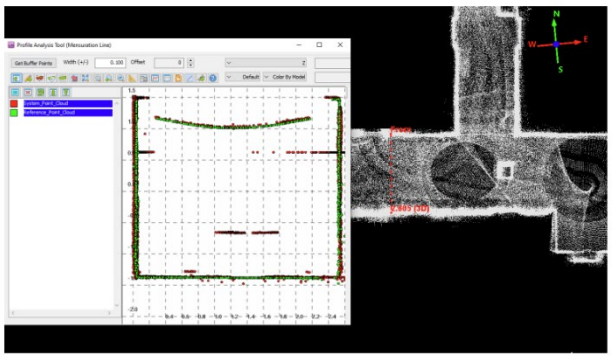

(a) System and Reference data profiles overlaid

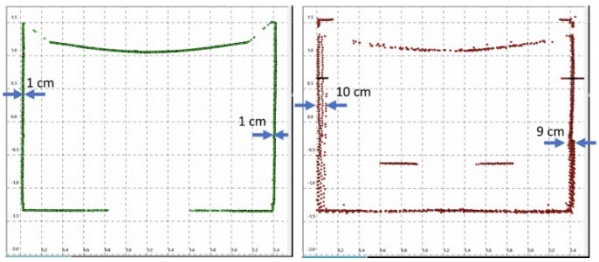

(b) Reference data profile (c) System data profile

Figure 15. System and reference Data Cross-sections Comparison

7. Discussion

The results highlighted the impact of MS Kinect data on point cloud generation. While the inclusion of MS Kinect data helped densify the point cloud, it also introduced noise and mechanical instability, affecting the quality of the resulting point cloud. The decision to conduct benchmarking and analysis using the point cloud generated solely from dual Lidar sensors is a pragmatic choice given these factors.

The reference TLS scans served as a vital reference dataset for benchmarking. The registration of these scans was successful, as evidenced by the low RMSE errors. This consistent reference point cloud was used as a baseline for comparison with the system-generated point cloud. The coregistration of the system and reference data was accomplished through the ICP registration process, which resulted in a mean registration error of 2 cm. This suggests an accurate coregistration process.

The examination of point distribution revealed that the reference data exhibited a consistent and well-distributed pattern, except for circular gaps caused by sensor limitations. In contrast, the proposed system point cloud did not show data gaps, but its density was less consistent compared to the reference dataset. Regarding data resolution, both the system and reference data exhibited clear features and details. However, the reference data, with its higher point density, provided sharper features.

One of the significant findings was related to data density. The reference data boasted significantly higher point density compared to the system data. This high point density in the reference data is vital for creating detailed 3D models and analysing small features or details in the environment.

The cross-section analysis revealed consistent ground and ceiling alignment with minimal misclosure. However, the system data exhibited variations in wall thickness compared to the reference data. This observation suggests that while the system data is relatively accurate and detailed, it may not match the precision and level of detail present in the reference data.

To sum up, the results demonstrate that proposed system can generate a point cloud suitable for various applications. The choice between using the system-generated data may depend on the specific project requirements. It's essential to consider the quality and characteristics of the data source when conducting geospatial data analysis and mapping tasks. Due to the low-cost sensors' accuracy and the noise inherited in those sensors, the system is recommended to be used in some applications that don’t require high accuracy but require prompt and instant data generation such as emergency response applications and disaster management.

A comprehensive comparison of the developed low-cost indoor mapping system against existing solutions available is presented. The objective is to evaluate the unique features and advantages of the developed system, particularly in the context of its lightweight, compact design, instant real-time processing capability, cost-effectiveness, and suitability for mass production for applications such as first responders and other emergency and commercial uses.

Lightweight and Compact Design: The developed system boasts a lightweight and compact design, ensuring easy integration into various vehicles and equipment. This feature enhances its portability and versatility, making it suitable for a wide range of applications such as underground/indoor search and rescue. While some market competitors may offer compact solutions, the developed system's emphasis on lightweight design sets it apart, allowing for deployment and operation in smaller, more agile vehicles and tight indoor spaces.

Real-Time Processing: A notable highlight of the proposed system is its capacity to perform real-time data processing, delivering instantaneous positioning and mapping outcomes. This feature proves particularly in scenarios where rapid decisionmaking is of utmost importance. Only a limited subset of existing systems provides real-time data acquisition capabilities. However, these solutions often demand substantial computational resources, whereas the developed system achieves realtime functionality with standard computer processing capacity.

Cost-Effectiveness and Mass Production: The proposed system is designed with cost effectiveness in mind, making it an attractive choice for mass production. This affordability factor is especially significant for applications involving first responders and commercial uses, where cost considerations play a crucial role. Some existing systems in the market can be cost-prohibitive due to their high-end features and pricing structures. The developed system's affordability and scalability position it favourably for widespread adoption and deployment.

8. Conclusion

This low-cost indoor mapping system was devised to tackle the challenges associated with capturing precise and comprehensive spatial data within intricate and confined indoor environments. The significance of the system lies in its lightweight and compact design, real-time data processing capabilities, and cost-effectiveness. These features distinguish it from existing solutions and position it as a compelling choice for situations where expeditious decision-making is of paramount importance.

The system's capability to gather spatial data in confined spaces holds immense value, particularly for applications in first responder scenarios, where rapid decision-making is imperative. As technology continues to progress, the compactness of the proposed system is anticipated to evolve further, enhancing its practicality for field tests across diverse scenarios. The real-time data processing capabilities constitute another critical feature. These capabilities bolster its appeal for scenarios where expeditious data acquisition and decision support are necessary.

In emergency response situations, first responders rely on real-time information to make critical decisions that can impact lives and property. The real-time processing capacity positions as an invaluable tool in such contexts. While acknowledging the strengths of the system it is equally imperative to recognize its limitations. The system's performance may exhibit variability across different indoor environments, prompting a recommendation for further evaluation in diverse settings as part of future work.

Ongoing advancements in sensor technology may influence the system's capabilities and cost-effectiveness, necessitating continual updates and enhancements. The systematic evaluation of the proposed system as detailed through the comprehensive benchmarking and analysis, provides valuable insights into the system's performance and the implications for geospatial data applications.

Nevertheless, the reference data in this research, boasting superior point density, yielded sharper and more precise feature representations. Of note, the research highlighted the significant disparity in point density between the reference data with a maximum density of 916,000 points per square meter and the system data with a maximum density of 14,000 points per square meter, with the former substantially outperforming the latter in this regard.

The reference stations collected from a static LiDAR and the time taken to collect and process the data is almost 10 times the time taken to collect and process the data by the proposed system. The Cross-sectional Analysis: It revealed that ground and ceiling alignment between the system and reference data was commendably consistent, with minimal misclosure, averaging only 2.5 cm. However, variability in wall thickness was observed in the system data when compared to the reference data, potentially signifying discrepancies in precision and level of detail.

In essence, this research underscores the importance of considering sensor integration and data quality in geospatial data acquisition. By shedding light on the trade-offs between different sensor configurations and their impact on data quality. Also, this research contributes to a deeper understanding of the choices available when selecting technology for specific applications. It underscores that achieving the right balance between cost, data quality, and real-time capabilities is essential for the successful deployment of geospatial systems. As technology advances, the prospects for geospatial data acquisition are boundless. The tools and methodologies developed here serve as a testament to the potential for innovation and the pursuit of efficiency in this critical field.

References

Chiang, K. W., Tsai, G.-J., and Zeng, J. C., 2021. Mobile Mapping Technologies. Urban Informatics, 439–465. Springer. doi: 10.1007/978-981-15-8983-6_25.

Di Filippo, A., Sánchez-Aparicio, L. J., Barba, S., Martín-Jiménez, J. A., Mora, R., and González Aguilera, D., 2018. Use of a wearable mobile laser system in seamless indoor 3D mapping of a complex historical site. Remote Sensing, 10(12), 1897. doi: 10.3390/rs10121897.

Elhashash, M., Albanwan, H., and Qin, R., 2022. A Review of Mobile Mapping Systems: From Sensors to Applications. Sensors, 22(11), 4262. doi: 10.3390/s22114262.

Li, L., Wang, R., and Zhang, X., 2021. A tutorial review on point cloud registrations: principle, classification, comparison, and technology challenges. Mathematical Problems in Engineering, 2021(1), 9953910. doi: 10.1155/2021/9953910.

Lv, J., Xu, J., Hu, K., Liu, Y., and Zuo, X., 2020. Targetless Calibration of LiDAR-IMU System Based on Continuous-time Batch Estimation. 2020 IEEE/RSJ International Conference on Intelligent Robots and Systems (IROS), 9968–9975. doi: 10.1109/IROS45743.2020.9341405.

Pomerleau, F., Colas, F., Siegwart, R., and Magnenat, S., 2013. Comparing ICP variants on real-world data sets. Auton Robot, 34(3), 133–148. doi: 10.1007/s10514-013-9327-2.

Quigley, M., et al., 2009. ROS: an open-source Robot Operating System. p. 6.

Sammartano, G., and Spanò, A., 2018. Point clouds by SLAM-based mobile mapping systems: accuracy and geometric content validation in multisensor survey and stand-alone acquisition. Applied Geomatics, 10(4), 317-339. doi: 10.1007/s12518-018-0221-6.

Velas, M., Spanel, M., Sleziak, T., Habrovec, J., and Herout, A., 2019. Indoor and outdoor backpack mapping with calibrated pair of velodyne LiDARs. Sensors, 19(18), 3944. doi: 10.3390/s19183944.

Xu, B., Liu, Z., Fu, Y., and Zhang, C., 2017. Research of cartographer laser SLAM algorithm. LIDAR Imaging Detection and Target Recognition 2017, SPIE, 49–57. doi: 10.1117/12.2292864.

Xue, F., Lu, W., Chen, Z., and Webster, C. J., 2020. From LiDAR point cloud towards digital twin city: Clustering city objects based on Gestalt principles. ISPRS Journal of Photogrammetry and Remote Sensing, 167, 418–431. doi: 10.1016/j.isprsjprs.2020.07.020.